HIGH-ENERGY ATTOSECOND-WIDTH ELECTRON DIFFRACTION SIMULATIONS

Honors Thesis
Submitted to the Faculty of the
Department of Physics and Astronomy of Vanderbilt University

April, 2013

by

DANIEL W. KIDD
Vanderbilt University

Primary Advisor:
Dr. Kálmán Varga

Committee of Examiners:
Dr. Steven Csorna
Dr. David Ernst
Dr. Thomas Weiler

VANDERBILT

Abstract

Electron microscopy has been the recent subject of molecular imaging due to the strength of the electrons' interaction with the target molecule making for a detailed pattern at a small scale.[1] To achieve the best 4D image of the target, one needs sufficient spatial and temporal resolution, the prior being an issue of using electrons in the keV regime as to achieve an optimally small deBroglie wavelength, and the latter being improved by the temporal width of the electron wave packet itself.[2] In order to image the motion of the electronic structure of the target molecule, this width must be within the attosecond regime. In this paper, we use the computational method of time-dependent density functional theory (TDDFT) to model our targets of Beryllium and the Nitrogen molecule, N_2, and an incoming electron wave packet with an energy of 1500 eV.

Contents

1 Introduction

1.1 Motivation

Recent advancement in the production of a high-energy attosecond-width electron source has been the primary motivation for this work.[3][4] Up until recently the major obstacle to overcome had been the achievement of an electron wave packet with a temporal width smaller than a few femtoseconds. It has been shown that by using two counter-propagating optical waves one can create an interference pattern which can then focus the femtosecond-width electron wave packet into individual attosecond wave packets by mechanism of ponderomotive forces (Fig. 1a).[4] These optical waves are aligned at an angle with respect to the traveling electrons (for many reasons including not interacting with the target molecules) and do not impare their speed. Simulations have shown a temporal width of as low as 20 attoseconds produced by this method (Fig. 1b). In order to successfully image the 4D motion of the excited states in a target, it is important that this temporal width be on the scale of under hundreds of attoseconds, as such is the regime at which electron motion occurs.[4]

Coulomb forces will cause repulsion, known as a space charge effect, between the electrons which hinders the overall electron flux that can be achieved which, in turn, hinders the intensity of the created diffraction pattern. An optimal number of 10 electrons per attosecond-width packet was found to minimize these effects while also maximizing the electron flux possible.[4] In this paper, we will only be using one electron in our wave packet.

Such an electron beam can be implemented into an experiment by use of a pump-probe method, in which an initial packet of electrons (pump) is used to excite the target molecule, and a second, well-timed, packet (probe) is used to analyze the changes in the system caused by the first interaction.[2][4] We have replicated the role of the pump

in this paper while using an unexcited Beryllium atom and an unexcited Nitrogen molecule as our targets. By use of TDDFT we are then able to visualize the resulting initial diffraction patterns as well as the motion of the electron density.

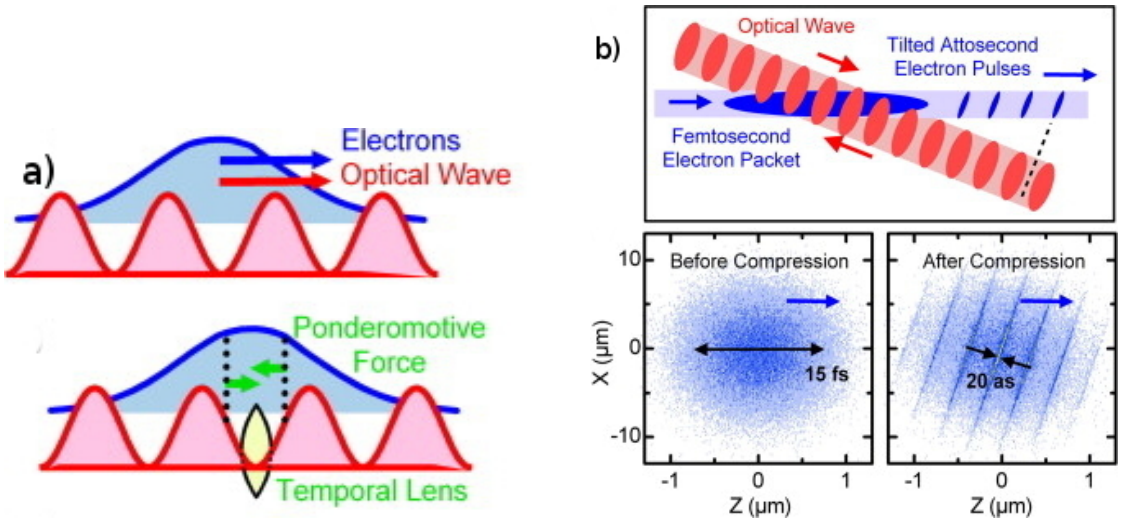

Figure 1: **a)** Two counter-propagating optical waves create an interference pattern that overlaps with the femtosecond width eletron wave packet. Ponderomotive forces then allow the creation of individual attosecond regime wave packets. **b)** The interfering optical waves are aligned at an angle so as not to interfere with the target. Slanted several-attosecond-width electron wave packets are created with the same original speed and direction.(Source: P. Baum and A. H. Zewail[4])

1.2 Outline

In section 2, a mathematical formalism is developed that describes the theoretical methods used in creating these simulations. First, the framework of density functional theory (DFT) as a method of finding the ground state of a system is demonstrated; then, TDDFT is looked into as the method of representing the density as a function of time thereby allowing the modeling of excited states. The implementation of a finite numerical grid is also discussed. We mention our use of complex absorbing potentials, describe our methods for integration and differentiation, and develop a modified kinetic

energy term for the Hamiltonian which allows for the propagation of high-momentum Gaussian wave packets.

In section 3, the conducted simulations are discussed in terms of the parameters used and the configuration of the system.

Section 4 then presents the resulting images created. Here we analyze the diffraction pattern created by Be and look at the detailed motion of the electron density of N_2 as it develops. We also look at the possiblity of electron capture in the N_2 simulation.

In conclusion, Section 5 summarizes the findings of our simulations along with room for possible improvement and proposed future extensions of this work.

2 Theory

2.1 Density Functional Theory

2.1.1 Hohenberg-Kohn Theorems

DFT is currently one of the most popular and promising modeling schemes for solving the Schrödinger equation for a system with interacting electrons. Such a modeling technique is required for this problem as an analytical solution to the many-electron Schrödinger equation is impossible due to the complexity of the the interaction between those bodies.[5] For use in systems where the Born-Oppenheimer approximation is assumed to be valid, the N-electron Schrödinger equation can be written as the following:

$$\left[-\sum_{i=1}^{N}\frac{\hbar^2}{2m}\nabla_i^2+\sum_{i=1}^{N}V\left(\mathbf{r}_i\right)+\sum_{i<j}^{N}U\left(\mathbf{r}_i,\mathbf{r}_j\right)\right]\Psi=E\Psi, \tag{1}$$

where

$$V\left(\mathbf{r}_i\right)=\sum_{A=1}^{N_A}\frac{Z_Ae^2}{|\mathbf{r}_i-\mathbf{R}_A|},\quad U\left(\mathbf{r}_i,\mathbf{r}_j\right)=\frac{e^2}{|\mathbf{r}_j-\mathbf{r}_i|}, \tag{2}$$

and Ψ is a function of all electron coordinates as well as their spins.

To traditionally solve this equation we would have to work with a $3N$ dimensional wavefunction. DFT, instead, uses the particle density, $n\left(\mathbf{r}\right)$

$$n\left(\mathbf{r}\right)=N\int\Psi^*\left(\mathbf{r}_1,\mathbf{r}_2,...,\mathbf{r}_N\right)\Psi\left(\mathbf{r}_1,\mathbf{r}_2,...,\mathbf{r}_N\right)d\mathbf{r}_2d\mathbf{r}_3...d\mathbf{r}_N, \tag{3}$$

with the goal of no longer working with many interacting particles but rather with ficticious, noninteracting particles within an effective external potential containing the effects of that interaction.

This concept is based around the two Hohenberg-Kohn Theorems:

Theorem 1. *The ground state density has a one-to-one correspondence with the poten-*

tial and thus uniquely determines all properties of the system, including the many-body wave function.

Theorem 2. *For any positive integer N and potential $v(\mathbf{r})$ there exists a density functional $F[n]$ (the HohenbergKohn functional) such that*

$$E_{(v,N)}[n] = F[n] + \int v_{ext}(\mathbf{r})\, n(\mathbf{r})\, d\mathbf{r} \tag{4}$$

obtains its minimal value at the ground-state density of N electrons. This minimum value of $E_{(v,N)}[n]$ is then the ground state energy of this system.

What this says is that by finding the ground state density, $n_0(\mathbf{r})$, we can derive the ground state energy and map the corresponding wavefunction, $\Psi_0[n_0]$.

2.1.2 Kohn-Sham Equation

We first go about implementing this method by use of Kohn-Sham energy partitioning. We define $F[n] = T_{KS}[n] + E_H[n] + E_{XC}[n]$ so that

$$E[n] = T_{KS}[n] + E_H[n] + E_{ext}[n] + E_{XC}[n], \tag{5}$$

where

-$T_{KS}[n] \equiv$ kinetic energy functional,

-$E_H[n] = \int\int \frac{n(\mathbf{r}')}{|\mathbf{r}-\mathbf{r}'|} d\mathbf{r} d\mathbf{r}' \equiv$ Hartree energy,

-$E_{ext}[n] = \int \epsilon_{ext}(\mathbf{r}) n(\mathbf{r}) d\mathbf{r} \equiv$ energy functional due to fixed ions and external fields,

-$E_{XC}[n] \equiv$ exchange-correlation energy.

Extrapolating on this concept we develop the Kohn-Sham equation

$$\left(-\frac{\hbar^2}{2m}\nabla_i^2 + V_H[n](\mathbf{r}) + V_{ext}[n](\mathbf{r}) + V_{XC}[n](\mathbf{r})\right)\phi_k(\mathbf{r}) = \epsilon_k\phi_k(\mathbf{r}), \tag{6}$$

where $n(\mathbf{r}) = 2\sum_{i=1}^{N}|\phi_i(\mathbf{r})|^2$ (The factor of 2 accounts for spin). This equation is commonly rewritten in terms of the Kohn-Sham potential, $V_{KS} = V_H + V_{ext} + V_{XC}$, as

$$\left(-\frac{\hbar^2}{2m}\nabla_i^2 + V_{KS}[n](\mathbf{r})\right)\phi_k(\mathbf{r}) = \epsilon_k\phi_k(\mathbf{r}). \tag{7}$$

It follows that ϕ_k must be solved self-consistently.

It is worth noting that V_{XC} is not known analytically for all systems. Well-fitting approximations exist that are used.[6][7] Other problems with using DFT include innacaurate band gap predictions and a lack of being able to describe excited states. For the latter, TDDFT can be used.

2.2 Time-Dependent Density Functional Theory

The concept behind TDDFT is described by the Runge-Gross theorem.[8]

Theorem 3. *For a many-body system described by an initial wavefunction, there exists a one-to-one mapping between the time-dependent potential(s) and the time-dependent density of the system.*

By use of this theorem, the time-dependent Kohn-Sham equation takes the following form:

$$i\hbar\frac{\partial\phi_k(\mathbf{r},t)}{\partial t} = \left(-\frac{\hbar^2}{2m}\nabla^2 + V_{KS}[n](\mathbf{r},t)\right)\phi_k(\mathbf{r},t), \tag{8}$$

where once again $n(\mathbf{r},t) = 2\sum_{k=1}^{N}|\phi_k(\mathbf{r},t)|^2$ and

$$V_{KS}(\mathbf{r},t) = V_{ext}(\mathbf{r},t) + V_H(\mathbf{r},t) + V_{XC}(\mathbf{r},t). \tag{9}$$

The exchange-correlation potential is simlarly unknown analytically as with DFT, however in TDDFT it is more complex and more poorly described. Creating better descriptions of $V_{XC}(\mathbf{r}, t)$ is an active area of research.[7][9]

2.3 The Finite Numerical Grid

2.3.1 Complex Absorbing Potentials

In our simulations, a numerical grid is implemented as a real-space approach for representing our system. This raises new challenges in correctly representing the dynamics being studied. A major example of this comes with the requirement that our wavefunctions reach zero at the boundaries of our finite grid, which leads to non-physical reflection. To solve this problem, we incorporate a complex absorbing potential (CAP) of the form $V_{CAP}(\mathbf{r}) = V_0(\mathbf{r}) + iW(\mathbf{r})$ where $V_0(\mathbf{r})$ is the original potential (before the implementation of the CAP) and $W(\mathbf{r})$ is an arbitrary smooth fucntion that is only non-zero near the boundaries of the grid and approaches infinity at those boundaries. This CAP absorbs the incoming wave so that it cannot reflect back.[5]

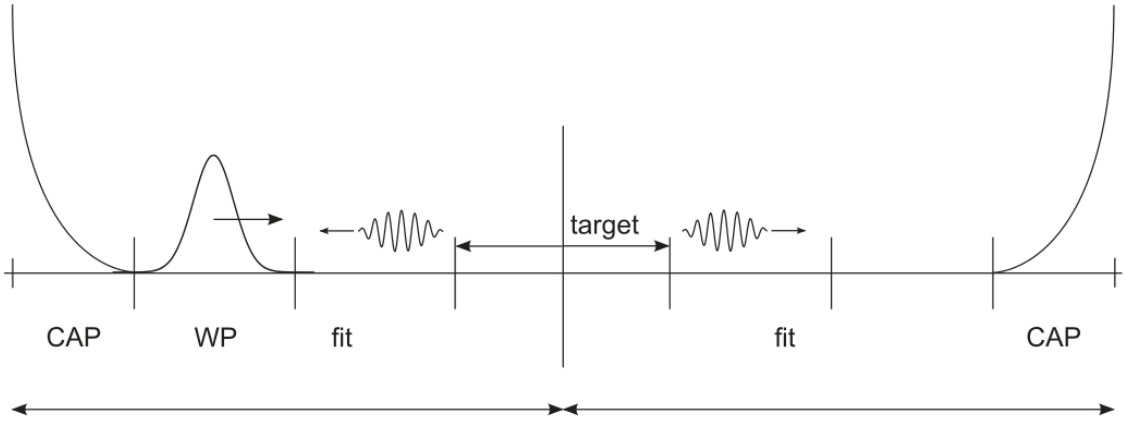

Figure 2: Complex absorbing potentials are placed at either end of this one dimensional schematic. These potentials prevent the wavefunctions from reflecting off the boundaries of the grid. (Source: K. Varga and J. Driscoll[10])

2.3.2 Numerical Methods Used

Using a numerical grid also means that we must use discrete-point methods for representing integrals and derivatives. For all integrals we use the 3-dimensional trapezoidal method[5]

$$\int_{\Omega} d\mathbf{r} f(\mathbf{r}) = h^3 \sum_{ijk} f(\mathbf{r}(i,j,k)). \tag{10}$$

For the calculation of first and second derivatives, we use a fourth order finite difference approach.[5] For example, a common task is to compute the kinetic energy acting on the wavefunction. This calculation incorporates the second derivative of the wavefunction and can be represented as the following:

$$\frac{\hbar^2}{2m}\nabla^2\psi(\mathbf{r}(i,j,k)) \approx \frac{\hbar^2}{2m}\sum_{n=-4}^{4} C_n \left[\psi(i+n,j,k) + \psi(i,j+1,k) + \psi(i,j,k+n)\right], \tag{11}$$

where $C_0 = -\frac{205}{72}$, $C_{\pm 1} = \frac{8}{5}$, $C_{\pm 2} = -\frac{1}{5}$, $C_{\pm 3} = \frac{8}{315}$, and $C_{\pm 4} = -\frac{1}{560}$.

These methods provide well-fit approximations for their respective yielded values in typical cases. However, as is shown in the following section, if the grid spacing is too large compared to drastic changes in the function being investigated, then these approximations become inaccurate.[5]

2.4 Propagation of High Energy Wave Packets

The 3D Gaussian wave packet, which is used as the representation of the pump-electron in this paper, can be described as the product of three 1D wave packets

$$\psi_G(\mathbf{r},t) = \phi_x(x,t)\phi_y(y,t)\phi_z(z,t), \tag{12}$$

where

$$\phi_a(a,t) = \left(\frac{\sigma_a}{\sqrt{\pi}(1+i\Omega_a t)}\right)^{1/2} \exp\left[-\frac{\sigma_a^2}{2}\frac{(a-\upsilon_a t)^2}{1+i\Omega_a t)}\right] \mathrm{e}^{ik_a(a-\upsilon_a t)}, \tag{13}$$

with $\upsilon_a = \hbar_a/m$, and $\Omega_a = \hbar\sigma_a^2/m$.

We propagate our wave packets by use of the time propagation operator

$$\Psi(\mathbf{r},t) = \mathrm{e}^{-iHt/\hbar}\Psi(\mathbf{r},0). \tag{14}$$

Here, H is the Hamiltonian operator. In order to apply this Hamiltonian operator within an exponential, we use the first four terms of a Taylor expansion to represent the time propagating factor[5]

$$\mathrm{e}^{-iHt/\hbar} \approx \sum_{n=0}^{4}\left[\frac{(-i\Delta t/\hbar)^n H^n}{n!}\right]. \tag{15}$$

This method provides accurate results for low wave packet energies (e.g. $\sim$50 eV) using a reasonably small grid spacing; however, if one increases the momentum of the wave packet and, therefore, the energy, then the de Broglie wavelength of the particle becomes very small, requiring a much smaller grid spacing to accurately describe it.[5] This necessity can be seen in the example depicted in equation 11. As stated above, if the function changes, or in this case, oscillates too rapidly within the scale of one grid spacing, then our value returned for the second derivative will be innacurate.

This problem can be worked around by separating the oscillatory term from the smooth Gaussian $\psi_G(\mathbf{r},t)$:[5]

$$\Psi(\mathbf{r},t) = \mathrm{e}^{i\mathbf{k}\cdot\mathbf{r}}\psi_G(\mathbf{r},t). \tag{16}$$

Rewriting the Schrödinger equation then obtains the following:

$$i\hbar\frac{\partial\psi_G}{\partial t} = H_k\psi_G, \tag{17}$$

where H_k is a modified Hamiltonian

$$H_k = \left[\frac{\hbar^2}{2m}(-\nabla^2 - 2i\mathbf{k}\cdot\nabla + \mathbf{k}^2) + V(\mathbf{r})\right]. \tag{18}$$

By substituting this modified Hamiltonian into the time propagation operator, we only propagate a smooth Gaussian $\psi_G(\mathbf{r}, t)$ while retaining all relevant information.[5] To reobtain the original wavefunction at time t we must only reapply the oscillatory factor to the smooth Gaussian at that time.

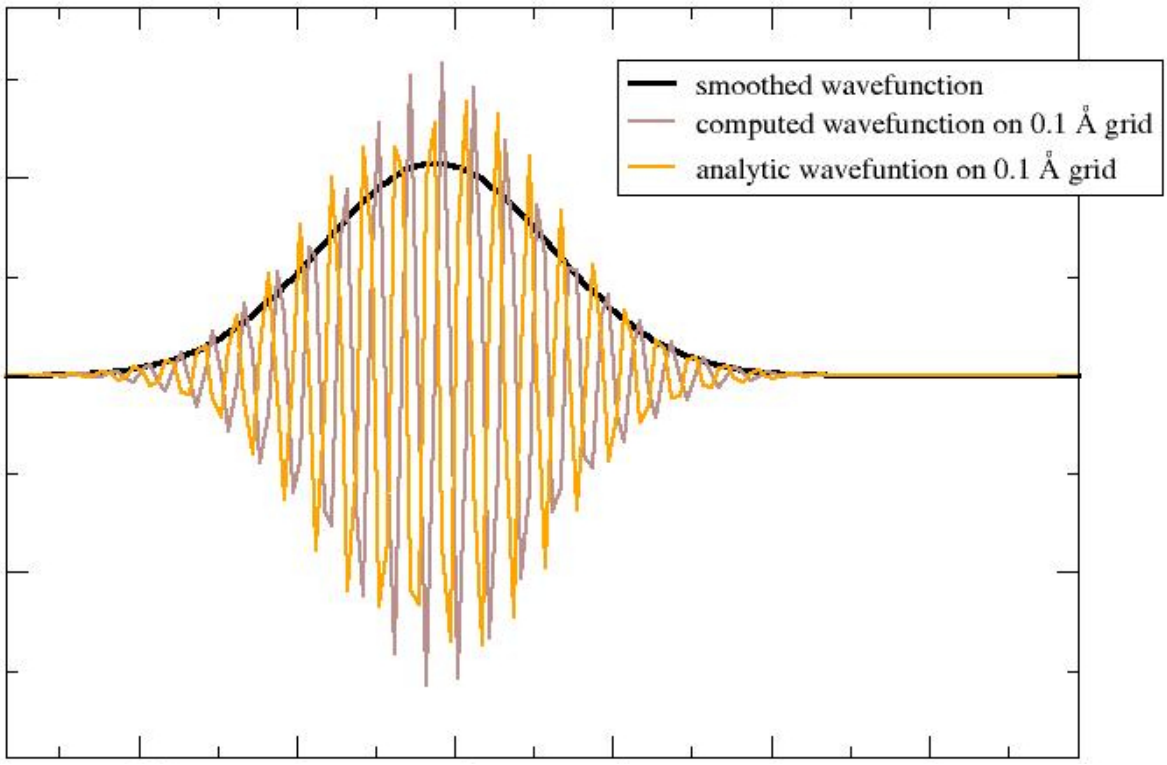

Figure 3: Representations of the wavefunction corresponding to an electron with energy 562 eV. The plotted analytical wavefunction Ψ (orange), the smoothed wavefunction ψ_G (black), and the plotted, reobtained solution for the wavefunction (grey) are each shown as represented on a grid with a spacing of 0.1 Å. Note that the reobtained and analytical wavefunction should agree given a small enough grid spacing.

3 System Configuration and Parameters

For our simulation we used a $30 \times 20 \times 20$ Å^3 box with a grid spacing of 0.125 Å. Our targets were placed at the center of the box (at coordinate (0,0,0)) while the incoming wave packet was initialized at a distance of -8 Å away in the x-direction and with a momentum of 13.06 eV $\cdot$ fs/Å (corresponding to 1500 eV and a de Broglie wavelength of 0.317 Å) towards them (see Fig. 4). The width of the wave packet was chosen to be 2 Å in x and 10 Å in both y and z in order to approximate a plane wave interaction. This width in the x-direction along with the above mentioned momentum corresponded to a temporal width of 8.7 as. Our complex absorbing potentials were non-zero at $x < -12$ Å and $12 < x$ Å as measured from the target.

This system was propagated with a time step size of 0.01 as over a total time of 400 as. By use of the previously discussed techniques we were able to calculate the 3D density of the system as a function of time. Because nucleonic motion occurs at the femtosecond scale, the nuclei are fixed and any molecular dynamical effects are ignored. It is also worth noting that the momentum of this electron wave packet corresponds with a speed of 0.08c, thus we are justified in ignoring any relativistic effects.

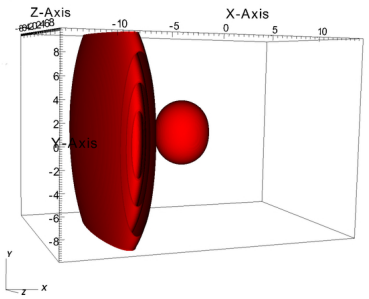

Figure 4: A plane wave approximation consisting of one electron is initialized at $x = -8$ Å and given positive momentum in the x-direction. The ground state electron density of N_2 shown here sits at the center of the box. A contour scheme is used to image the 3D density throughout this paper.

4 Results

4.1 Beryllium

Fig. 5 shows the results of our model for Beryllium. The electron wave packet can be seen passing through the atom and being absorbed by our CAP afterwards. Note that due to a lack of CAPs on either the y or z axes, there is some minimal reflection within our wave packet off of these boundaries. This effect is slight enough that it does not cause any unwanted behavior in the created excited states of the target.

We observed the created diffraction pattern much as an experimental screen would by taking a slice of the density at $x = 8$ Å. Expected time-dependent circular rings were produced (Fig. 6).

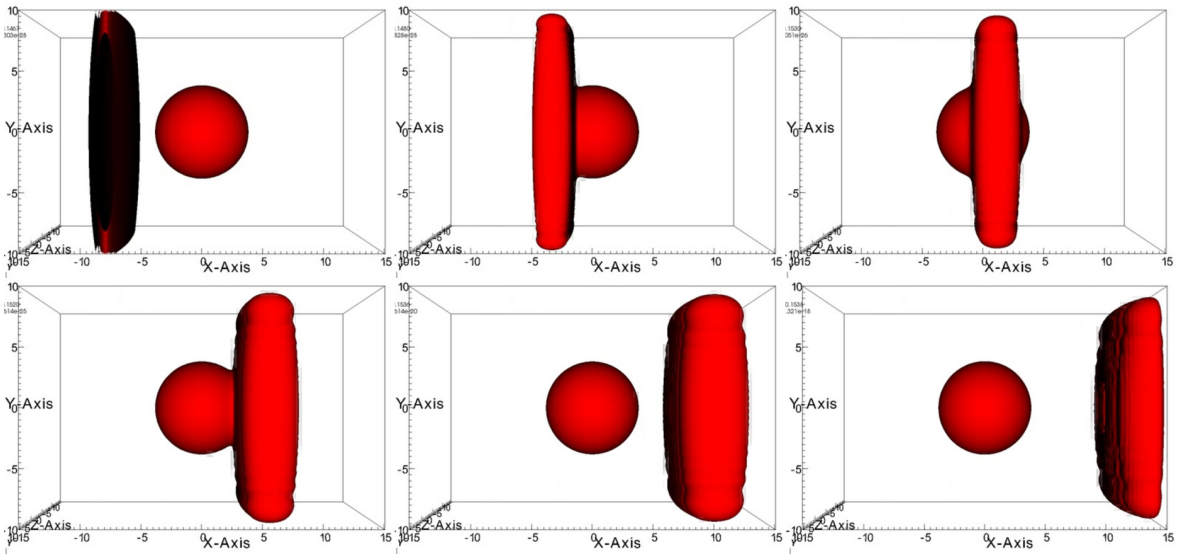

Figure 5: Frames of the 3D density taken at increments of 20 as for a total duration of 100 as for Be. (an order of top-left to bottem-right is used throughout this paper)

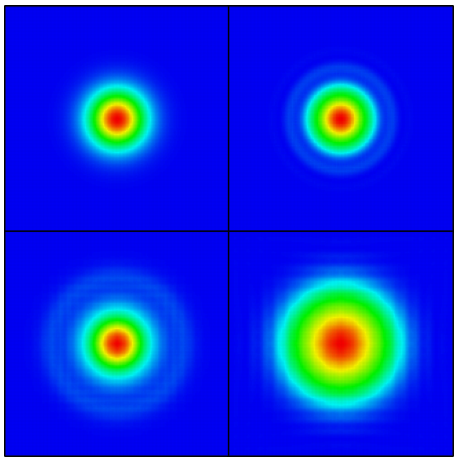

Figure 6: Frames of the 2D density slice taken at $x = 8$ Å in increments of 100 as during 400 as for our Be simulation. Note that in this visualization method the density scale is normalized in each frame.

4.2 Nitrogen Molecule

Next, in Fig. 7, the electron density is shown through the first 120 as for N_2. First, we can notice the created diffraction pattern within the electron wave packet after impact (Fig. 8). The rectangular wave-like properties of the wave packet are a product of the above mentioned reflection from the bounderies; however, the circular diffraction pattern is evident. We also investigated any possible electron capture by analyzing the total number of electrons after the plane wave had been absorbed. The difference of this value and the expected number of electrons in N_2 came to be only 6×10^{-7} electrons, which is small enough to be considered numerical noise; therefore, we conclude that there is no electron capture or ionization for that matter. Lastly, we can determine that any back scattering effects are minimal as they only arise in our vizualizations with very small density values and, therefore, in effect, have only a very low probability of occuring.

Next, to examine the excited states of the target molecule, we took the difference

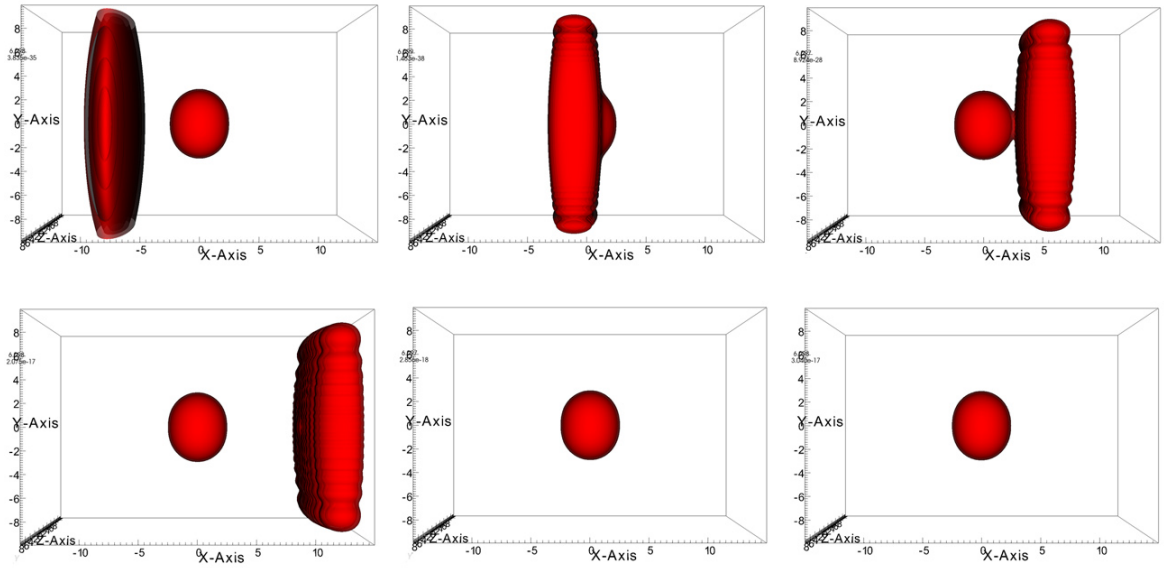

Figure 7: Frames of the 3D density taken at increments of 30 as for 120 as.

of the density at each time frame and the original density at $t = 0$. This then, of course, created positive values for where the electron density went, and negative values for where the electrons were. Plotted together, these new images show a detailed depiction of the electron motion in the excited states of the Nitrogen molecule (Fig. 9).

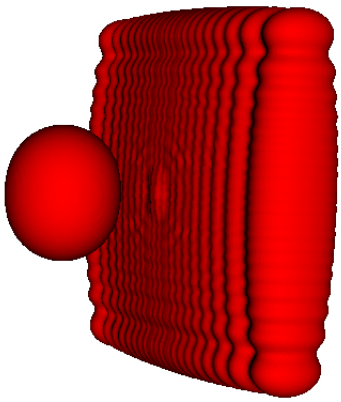

Figure 8: The circularly symetric diffraction pattern can be seen within the wave packet after its collision with the N_2 molecule.

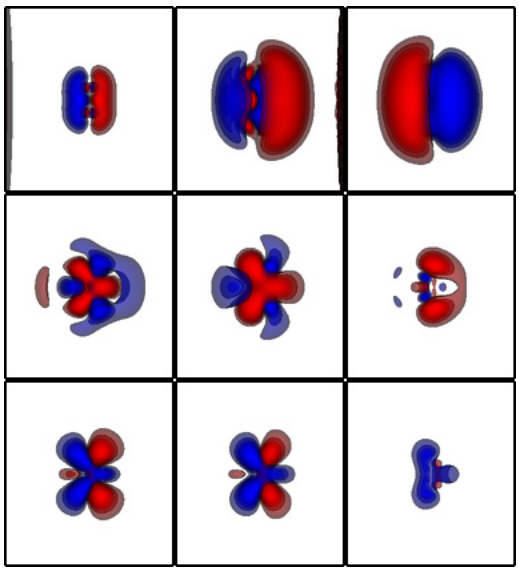

Figure 9: The difference in the density at $t = 10$ through $t = 400$ and the ground state density taken at increments of 50 as depicted as either positive values (red) or negative values (blue). The first frame is omitted as it is completely cancelled out and appears blank.

5 Summary

We have successfully modeled a high-energy attosecond-width electron diffraction experiment using TDDFT and a modified Hamiltonian necessary for depicting a highly oscillatory wavefunction on a numerical grid. Through this model we have visualized the diffraction pattern created by a target of Beryllium, and the excited states of the Nitrogen molecule replicating the aftermath of the pump in a pump-probe experiment. Moreover, we have validated that the electron count for N_2 during such a pump-electron interaction stays constant, thereby illustrating that there is no electron capture or ionization taking place.

An improvement to the methods shown here could be the use of a larger box for our system, in remark to the noise created in our wave packet resulting from its close proximity to the boundaries of the grid. Similarly CAPs for each of these remaining sides of the box would eliminate such an effect, given that the box is large enough to allow a CAP that does not overlap with the wave packet itself. As stated above, this effect has no effects in our simulations; however, if we were to replicate a diffraction pattern created by the probe in a pump-probe experiment, we would want a clean image for comparison with experimental data. Obviously improvement also comes with smaller grid spacings and time steps at the cost of computational time.

As alluded to above, a possible future extension of this work would be to include the probing electron and an analysis of its created diffraction pattern. There is also the capability in DFT to include laser excitation (as an oscillating electric field) which could be used to study the created diffraction patterns of target molecules under such conditions.

References

[1] D. J. Flannigan and A. H. Zewail, 4D electron microscopy: principles and applications, Accounts of Chemical Research 1828–1839 (2012).

[2] A. H. Zewail and J. M. Thomas, *4D Electron Microscopy: Imaging in Space and Time* (Imperical College Press, 2010).

[3] P. Baum and A. H. Zewail, Attosecond electron pulses for 4D diffraction and microscopy, Proceedings of the National Academy of Sciences 18409–18414 (2007).

[4] P. Baum and A. H. Zewail, 4D attosecond imaging with free electrons: diffraction methods and potential applications, Chemical Physics 2 – 8 (2009).

[5] K. Varga and J. Driscoll, *Computational Nanoscience* (Cambridge University Press, New York, 2011).

[6] H. Eschrig, *The Fundamentals of Density Functional Theory* (Edition am Gutenbergplatz, 2003).

[7] J. P. Perdew and A. Zunger, Self-interaction correction to density-functional approximations for many-electron systems, Phys. Rev B 5048–5079 (1981).

[8] M. Marques, C. Ullrich, F. Nogueira, et al., *Time-Dependent Density Functional Theory* (Springer, 2006).

[9] P. Elliott, K. Burke, M. H. Cohen, and A. Wasserman, Partition Density Functional Theory, Phys. Rev. A 024501 (2010).

[10] J.-A. Yan, J. A. Driscoll, B. K. Wyatt, et al., Time-domain simulation of electron diffraction in crystals, Phys. Rev. B 224117 (2011).

[11] A. Paarmann, M. Gulde, M. Müller, et al., Coherent femtosecond low-energy single-electron pulses for time-resolved diffraction and imaging: A numercial study, J. Appl. Phys. **112**, 113109 (2012).